

Geophysical Research Letters

Supporting Information for

Reorganized atmospheric circulation during the Little Ice Age leads to rapid Southern California deoxygenation

Yi Wang¹, Ingrid L. Hendy¹

¹Department of Earth and Environmental Sciences, University of Michigan, Ann Arbor, MI, USA

Contents of this file

*Text S1 to S5
Figure S1 to S7
Table S1 to S2*

Introduction

The supplementary Information provides additional background on the Santa Barbara Basin core sites (Fig. S1), ventilation sources of the Southern California oxygen minimum zone (OMZ, Text S1), detailed descriptions of the Last Millennium Reanalysis data and analysis (Text S2, Fig. S2 and S3), rationale of using Ba_{excess} as an indicator of relatively oxygenated conditions (Text S3), and calculations of the OMZ intensification/recovery rates (Text S4, Fig. S4). Text S5 justifies the use of in-phase/out-of-phase relationships between the Santa Barbara Basin (Wang et al., 2019) and Pescadero Slope (Tems et al., 2016) $\delta^{15}N$ records to track the Eastern Tropical North Pacific denitrified water transport. Figure S6 shows a rolling correlation between the Santa Barbara Basin (Wang et al., 2019) and Pescadero Slope (Tems et al., 2016) $\delta^{15}N$ records discussed in the main text Section 4 and Figure 3. Figure S7 is an extension of Figure 3 in the main text that shows the proxy record comparison to the first millennium. Additionally, we present elemental compositions of sediment reference materials (Table S1) and the core SPR0901-03KC as separate data tables (Table S2).

Text S1. Remote ventilation sources of the Southern California OMZ

Intermediate water masses ventilating the southern California OMZ include cold and well oxygenated North Pacific Intermediate Water (NPIW), as well as the warm and low oxygen

Equatorial Pacific Intermediate Water (EqPIW). As the densest water mass formed in the North Pacific, NPIW (potential density $\sigma_\theta = 26.7\sim 26.9 \text{ kg m}^{-3}$, 300 – 800 m water depth, Reid (1965); You (2003)) forms in the Mixed Water Region between the Kuroshio Extension and the Oyashio Fronts (Miyao and Ishikawa, 2003; Talley, 1993; Yasuda, 1997; You, 2003). NPIW primarily ventilates in the Sea of Okhotsk (Fig. 1), where coastal polynya development due to winter sea ice brine injection on the northern and northwestern shelf leads to well-oxygenated dense shelf water (DSW) formation (Shcherbina et al., 2004a; Shcherbina et al., 2004b; Talley, 1993; Watanabe and Wakatsuchi, 1998). The Gulf of Alaska may be an additional NPIW source region in winter but its contribution is minor (~10%) and restricted to upper NPIW (You et al., 2000; You et al., 2003).

NPIW ventilation induced by Sea of Okhotsk ice formation is closely associated with atmospheric circulation (e.g., position and intensity of the Aleutian Low [AL] and Siberian High [SH]) that determines both wind direction and stress (Kimura, 2004; Martin et al., 1998; Parkinson, 1990; Tachibana et al., 1996). Increased sea ice brine rejection (ventilation) usually corresponds to strong offshore (northerly/northwesterly) winds under deepened AL centered in the northeastern Pacific and/or intensified SH in the far-east Asia (Parkinson, 1990; Tachibana et al., 1996), because the strong offshore winds facilitate polynya production in the sea leading to intermediate water formation. Westward/weakened AL and SH that lead to easterlies and reduced wind stress, on the contrary, are usually linked with milder sea ice conditions and less ventilation in the Sea of Okhotsk (Fig. 1).

EqPIW, an intermediate water mass from tropics, is a mixture of heavily modified Antarctica Intermediate Water (AAIW) and upwelled Pacific Deep Water forming in the western equatorial Pacific (Bostock et al., 2010). EqPIW is then transported towards the eastern equatorial Pacific (EEP) via the Equatorial Undercurrent, where dissolved oxygen in the EqPIW is further consumed due to high primary productivity driven by extensive equatorial upwelling. This low-O₂ subsurface water mass is then advected north to the Southern California via the California Undercurrent (CUC) (Fig. S1).

Text S2. Last Millennium Reanalysis data

The Last Millennium Reanalysis project applies an ensemble data assimilation approach (DA), which incorporates information from proxy reconstructions into model simulated data that serve as prior expectations (Hakim et al., 2016; Tardif et al., 2019). The prior ensemble in each Monte Carlo realization was drawn from 100 random years in the Community Climate System Model version 4 (CCSM4) Last Millennium simulation (Tardif et al., 2019; Taylor et al., 2011). The proxy database used is the most extensive high-quality temperature-sensitive records currently available (PAGES 2k Consortium, 2017). Regression-based proxy system models (PSM) for different proxy categories (e.g., tree ring width, coral $\delta^{18}\text{O}$) were applied to estimate the assimilated proxy values from the prior climate variables (e.g., temperature from model simulations), and an ensemble Kalman filter was used to update the prior ensemble (Hakim et al., 2016; Steiger et al., 2014; Tardif et al., 2019). A cut-off length scale of 25000 km was applied with covariance localization in order to avoid spurious covariance with remote records (Hamill et al., 2001). The annual data product is presented on a $2^\circ \times 2^\circ$ grid and each variable contains 13 LMR Monte Carlo reconstructions. The grand mean was validated against gridded instrumental analyses (Tardif et al., 2019). A broad region of 50 – 65°N and 135 – 170°E was chosen to generate time series of spatially averaged

climate variables in the Sea of Okhotsk to investigate site specific responses to CE climate change (Fig. 4 and S3).

The interval of 1550 – 1750 CE was targeted in the LMR following elevated sedimentary Mo and Re enrichments in the SBB record to better understand the forcing mechanism of this interval. A dipole pattern over the high-latitudes is indicated in the 1550 – 1750 CE sea level pressure (SLP) anomaly (Fig. 4). Negative SLP anomalies were found over the northern Europe, Siberia, Barents Sea, Sea of Okhotsk, Japan Sea, and the Gulf of Alaska, whereas positive SLP anomalies were prevalent over the Greenland and Canadian Arctic Archipelago. Similarly, negative 500 hPa geopotential height anomalies prevailed over the Gulf of Alaska, Siberia, northern Europe and the Sea of Okhotsk, with a slightly positive anomaly over central Pacific and the northwest America (Fig. S2). Precipitation rates, however, only show minor anomalies over the Okhotsk Sea region during 1550 – 1750 CE, suggesting that precipitation-induced salinity change and surface water buoyancy change should be minor (Fig. S3).

Text S3. Redox control on sedimentary Ba preservation

Ba_{EF} is often used as a productivity indicator for sediments dominated by biogenic input and with minimal terrestrial influences (Eagle et al., 2003). Ba precipitates as barite ($BaSO_4$) on falling particles in the water column and then buried if porewaters are oxygenated (Bishop, 1988; Dymond et al., 1992; Ganeshram et al., 2003; Gingele et al., 1999; McManus et al., 1994; Paytan and Griffith, 2007). Although stable in oxygenated environments, authigenic barite ($BaSO_4$) can be dissolved to release as free Ba^{2+} in sulfidic porewaters where sulfate reduction occurs and sulfate serves as an electron acceptor in organic carbon (OC) decay (Griffith and Paytan, 2012; Hendy, 2010; McManus et al., 1998; Torres et al., 1996; Von Breymann et al., 1992). Although barite dissolution in sulfidic thus compromises the original productivity signal in the Ba_{excess} record, the described diagenesis can provide an additional redox information to support redox-sensitive metal proxies. Depleted oxygen and sulfate reduction occurs within the top several millimeters in the central SBB porewaters, and free HS^- usually accumulates within 5 cm below the sediment-water interface (SWI) (Kuwabara et al., 1999; Raven et al., 2016; Reimers et al., 1996). Thus, typically authigenic barite is dissolved in the SBB porewaters, releasing free Ba^{2+} to the ambient waters such that only lithogenic-bound Ba remains in the sediments. However, Ba shows a statistically significant correlation ($r = 0.57$, $p < 0.05$) with previously published total organic carbon (TOC) in SPR0901-03KC, which has shown to be a robust export productivity proxy in this core (Wang et al., 2019). High frequency variability in Ba_{excess} can thus be explained by export productivity in SBB even though sedimentary Ba remobilization occurred under sulfate reduction. However, the broad increase in Ba_{excess} between 1250 and 1550 CE above the lithogenic background corresponds to low $Metal_{EF}$ (Fig. 2b), suggesting this interval was associated with increased barite preservation under relatively more oxygenated conditions.

High Ba_{excess} values occur at 1090 CE, corresponding to a local minimum of redox-sensitive $Metal_{EF}$. Although it is possible that this peak is associated with barite preserved during an abrupt oxygenation interval in SBB during 1075 – 1100 CE, barite dissolution increases below this peak as evidenced by a decreasing Ba_{excess} trend downcore. Additionally, the peak at 1090 CE is located within the sulfate depletion zone range (~100 – 150 cm below the SWI) (Berelson et al., 2005; Harrison et al., 2009; Reimers et al., 1996). Thus, it is more likely that this peak is the result of diagenetic barite (Hendy, 2010) precipitated from Ba^{2+} that diffused during sulfate reduction below the SWI and SO_4^{2-} diffusing from HS^- oxidation at the SWI (Torres et al., 1996; Von Breymann et al., 1992). This peak stopped migrating at 1100 CE either during the oxygenated interval, or as a result

of the earthquake-induced turbidite at 1108 CE (Du et al., 2018). Similarly, the maximum Ba_{excess} values found in the upper 5 cm of SPR0901-04BC are likely associated with a modern re-precipitation peak of barite that is currently still migrating toward the SWI (Fig. 2a). Diagenetic barite peaks have been widely reported in continental margin records but usually occur in more deeply buried sediments as the porewaters of these margins are generally better oxygenated than in SBB (Hendy, 2010; McManus et al., 1998; Riedinger et al., 2006; Torres et al., 1996).

Text S4. Southern California OMZ intensification and relaxation rate calculation

SBB bottom waters are consistently bathed by low-oxygen bottom waters that facilitate *Re* enrichments, while *Mo* enrichments indicate a more sulfidic environment with lethal effects on benthic macro/mega-organisms. Mo_{EF} can thus provide a qualitative estimate of OMZ intensification and relaxation rate as Mo_{EF} responses to bottom water oxygenation may not be linear. Uneven sampling of the core (denser sampling in the MCA and LIA) may have smoothed out high-frequency OMZ oscillations for intervals with lower sampling resolution, and thus a 5-point Mo_{EF} moving average, which suppresses high-frequency oscillations and highlights multidecadal variability was used to identify OMZ intensification/relaxation intervals. The beginning and end of each OMZ intensification/relaxation interval was determined from the turning points. Each interval has at least 5 data points to allow OMZ expansion/relaxation rate calculation using a linear least-square regression (Fig. S4a). Only intervals with statistically significant correlation coefficients (5% significance level) are reported. Eight intervals of OMZ intensification and six intervals of OMZ relaxation were identified in the 2000-year record (Fig. S4b). Another OMZ intensification interval was also identified in the post-Industrial sedimentary record (1927–1969, Fig. S4b). The most recent intensification period (2000–2007) was not included as only 4 data points in the record span the interval and more data would be needed to confidently assess the rate of change. We further calculated the magnitude and frequency of *Mo* variability using Mo_{EF} rate of change ($\Delta Mo_{\text{EF}}/\text{year}$) from the derivative between the adjacent data points (Fig. S4c). A number of intervals — 520 – 780, 920 – 1160, and 1480 – 1840 CE — show rapid OMZ oscillations with $\Delta Mo_{\text{EF}}/\text{year}$ amplitude exceeding 1 standard deviation (Fig. S4c), suggesting that high-frequency and large magnitude of OMZ oscillations are not uncommon and occurred sporadically during the past 2000 years.

Text S5. Sedimentary $\delta^{15}\text{N}$ as a tracer of southern denitrified water transport to the Southern California Margin

The sedimentary $\delta^{15}\text{N}$ ($\delta^{15}\text{N}_{\text{sed}}$) records from Southern California have been employed as an indicator of mixing between the high- $\delta^{15}\text{N}$ denitrified waters in the Eastern Tropical North Pacific (ETNP) advected via the California Undercurrent (CUC), and the high-nutrient subarctic waters transported via the California Current (Altabet et al., 1999; Kienast et al., 2002; Liu and Kaplan, 1989) (Tems et al., 2015; Wang et al., 2019). A two end-member mixing model between the northern and southern sourced waters was proposed by Tems et al., 2015, where the reduced $\delta^{15}\text{N}_{\text{sed}}$ difference ($\Delta\delta^{15}\text{N}_{\text{sed}}$) between the Southern California margin site (e.g., Santa Monica Basin) and the Pescadero Slope (representing ETNP denitrification) indicates stronger southern water transport from ETNP. To test this mixing model in the SBB, we used $\delta^{15}\text{N}_{\text{sed}}$ from an SBB box core (SPR0901-04BC, 34°16.895'N, 120°02.489'W, 588-m water depth), and observed salinity at the core of CUC ($\sigma_\theta = 26.4\text{--}26.5$, Gay & Chereskin, 2009) from the California Cooperative Oceanic Fisheries Investigations (CalCOFI) station 81.8 46.9 (center of SBB, 34°16'29.64"N, 120°1'30"W) during the last 50 years. However, there was no statistically significant correlation ($R^2 = 0.2168$, $p = 0.06$) between the $\Delta\delta^{15}\text{N}_{\text{sed}}$ of the two sites and SBB salinity (Fig. S5). Additionally, the Pescadero slope and Santa Monica Basin $\delta^{15}\text{N}_{\text{sed}}$ show general in-phase variability throughout the record (Tems et

al., 2015), whereas out-of-phase oscillations occurred for the SBB and Pescadero slope records during the Common Era (Wang et al., 2019). $\delta^{15}\text{N}_{\text{sed}}$ in SBB is always lower than that from the Pescadero slope, consistent with greater mixing as CUC water moves poleward along the North American margin. When ETNP denitrification weakens (low Pescadero $\delta^{15}\text{N}_{\text{sed}}$) but SBB $\delta^{15}\text{N}_{\text{sed}}$ increases, the out-of-phase relationship could then reduce the $\Delta\delta^{15}\text{N}_{\text{sed}}$ between the two sites (e.g., 1740–1820 CE, Fig. 3 and S6). This low $\Delta\delta^{15}\text{N}_{\text{sed}}$ signal generated from out-of-phase variability contrasts from the low $\Delta\delta^{15}\text{N}_{\text{sed}}$ values generated under in-phase variations observed in Tems et al., 2015.

We thus used a 25-point rolling correlation that calculates the correlation coefficient of the two records continuously (Fig. S5) to distinguish in-phase/out-of-phase relationships. Although the rolling correlation could be affected by individual data points and age model differences, we can still evaluate the overall change of positive/negative correlations. When a statistically significant in-phase/positive correlation is observed, the southern denitrified water influence is stronger; whereas out-of-phase/negative correlation indicates weakened influences from the ETNP (Wang et al., 2019). This framework of in-phase/out-of-phase relationship is validated with a statistically significant correlation between the modern CalCOFI salinity observations and $\delta^{15}\text{N}_{\text{sed}}$ from the box core 04BC was found (Wang et al., 2019). Statistically significant positive correlation is observed at 1000, 1200–1520, and \sim 1760, while anti-correlation is shown in \sim 960, 1080, 1260, 1320, 1560, 1680–1720, and 1780–1820. Notably a transition from sustained in-phase to frequent out-of-phase relationship occurred at \sim 1540, indicating a possible weakening of ETNP denitrified water transport.

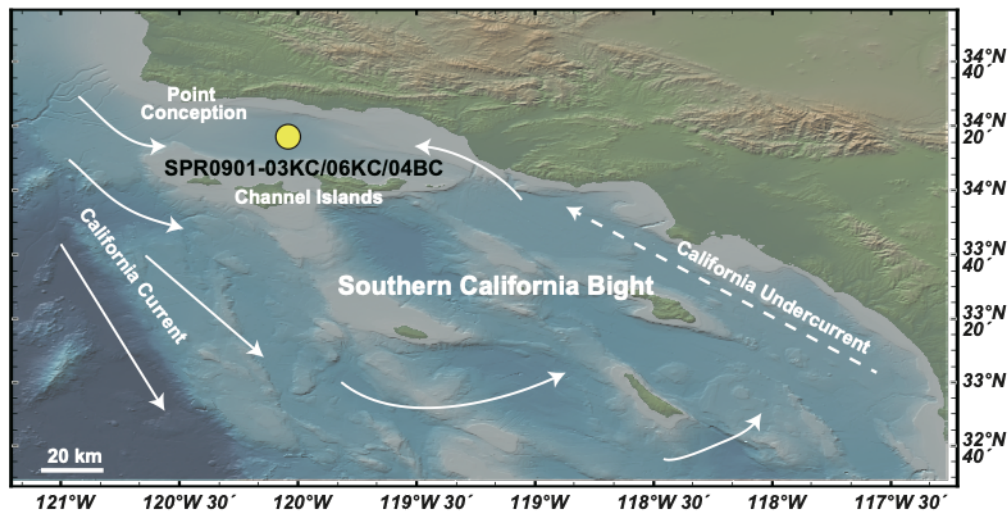


Figure S1. Ocean circulation associated with the Santa Barbara Basin. The cores SPR0901-03KC, SPR0901-03KC, and SPR0901-04BC are located within the yellow circle. White arrows show the currents and the circulation pattern is modified from Hickey (1992). The basemap was generated using the GeoMapApp (<http://www.geomapapp.org>, Ryan et al., 2009).

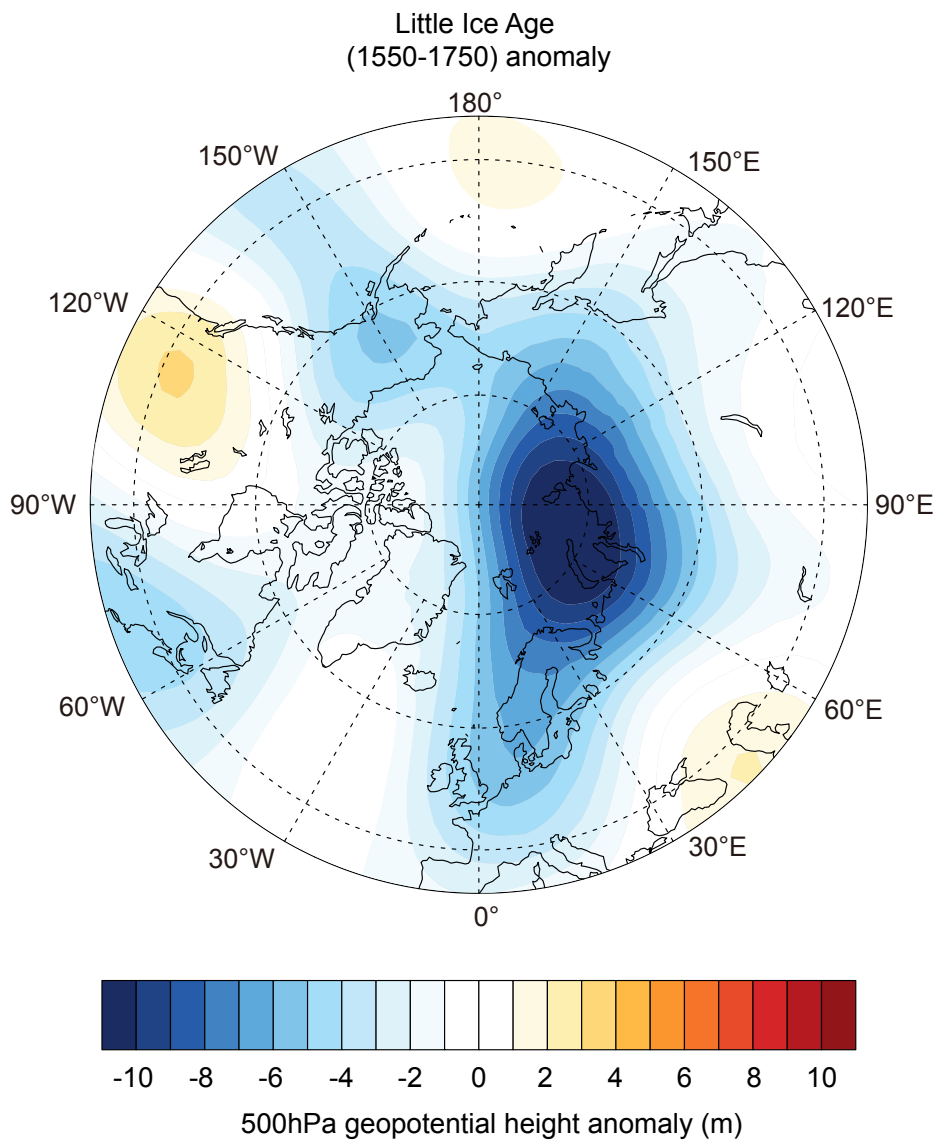


Figure S2. 500hPa geopotential height anomaly (m) of the late Little Ice Age (1550–1750 CE) with respect to the pre-1850 mean.

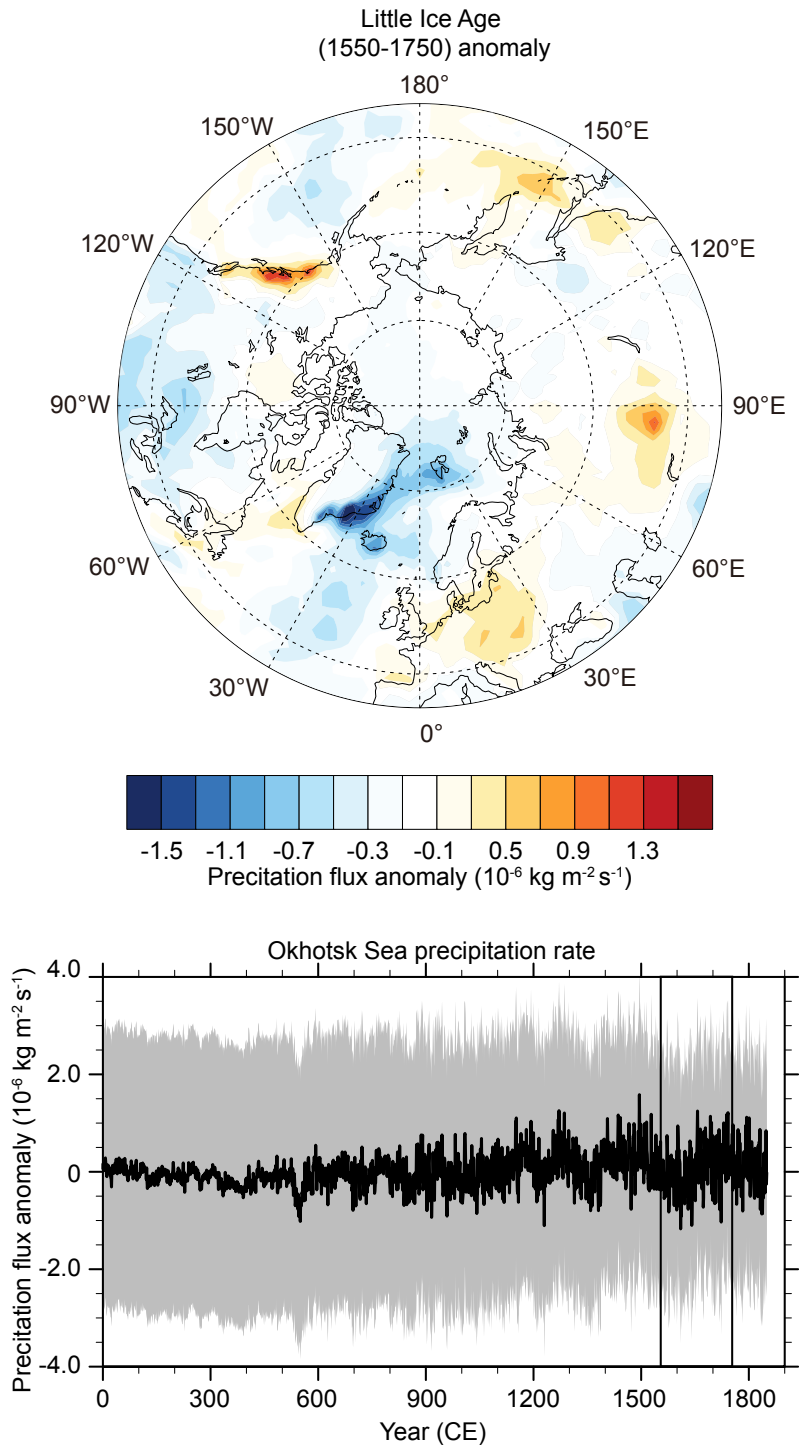


Figure S3. Upper panel: Precipitation rate anomaly of the late Little Ice Age (1550–1750 CE) with respect to the pre-1850 mean. Lower panel: Area weighted precipitation rate anomaly time series over the Sea of Okhotsk (50–65°N, 135–170°E). The 1550–1750 CE interval is outlined by the black rectangle.

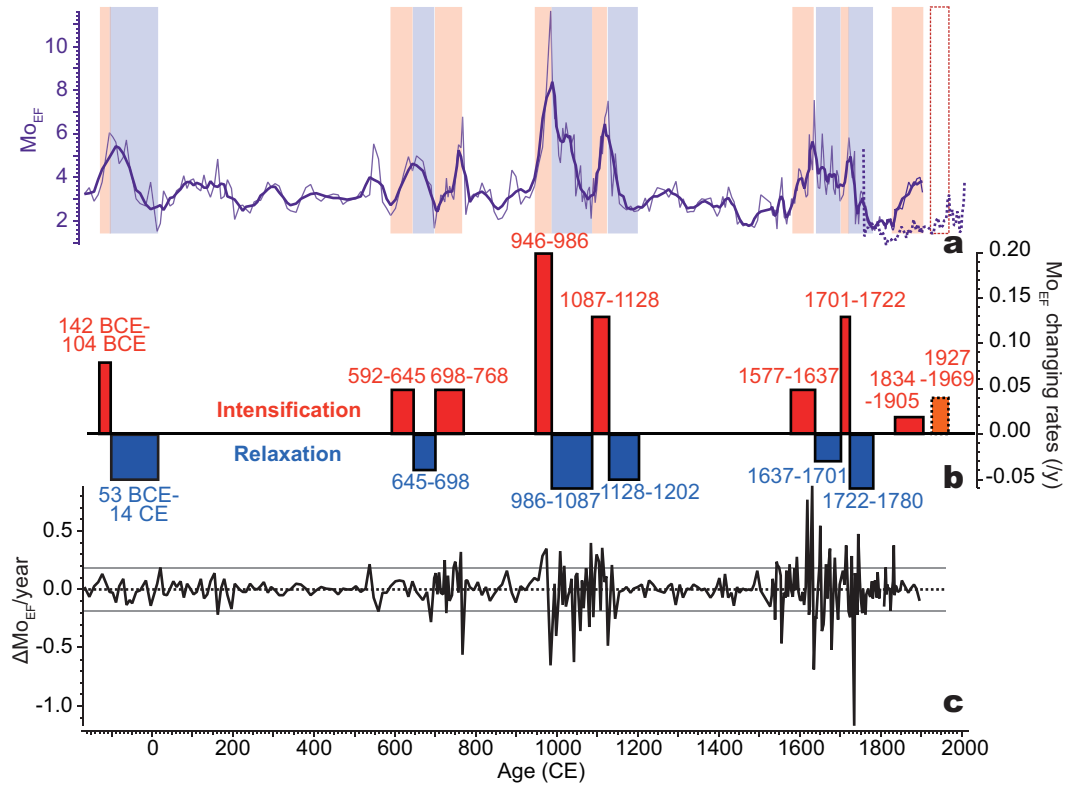


Figure S4. Oxygen minimum zone intensification and relaxation rates. (a) Mo_{EF} from SPR0901-03KC (thin solid purple line) curve with the 5-point running mean (thick solid purple line) and from the core SPR0901-04BC (purple dashed line) spanning the post-Industrial time interval. Identified oxygen minimum zone intensification and relaxation intervals are denoted as red and blue bars, respectively. The selected 04BC interval for OMZ intensification rate calculation is denoted by a dashed rectangle outlined in red. (b) Calculated OMZ intensification/recovery rates based on the least-square linear regression of Mo_{EF} during the intervals identified in (a). Ages of the identified intervals are labeled. The OMZ intensification rate of 03KC is outlined by a solid line, while 04BC is outlined by a dashed line. (c) Changing rates of Mo_{EF} between the two adjacent points. The two horizontal solid lines represent the 1SD envelope.

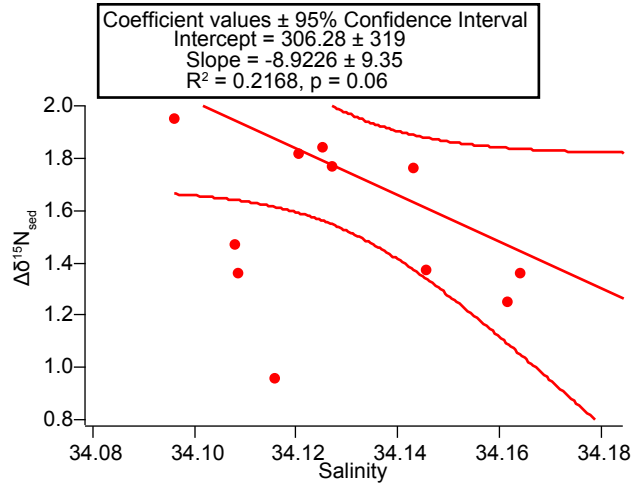


Figure S5. Salinity (CUC core [$\sigma_\theta = 26.4\text{--}26.5$] observations from CalCOFI during 1953–2005) vs. $\Delta\delta^{15}N_{sed}$ of the Santa Barbara Basin and the Pescadero Slope (Tems et al., 2015, Wang et al., 2019).

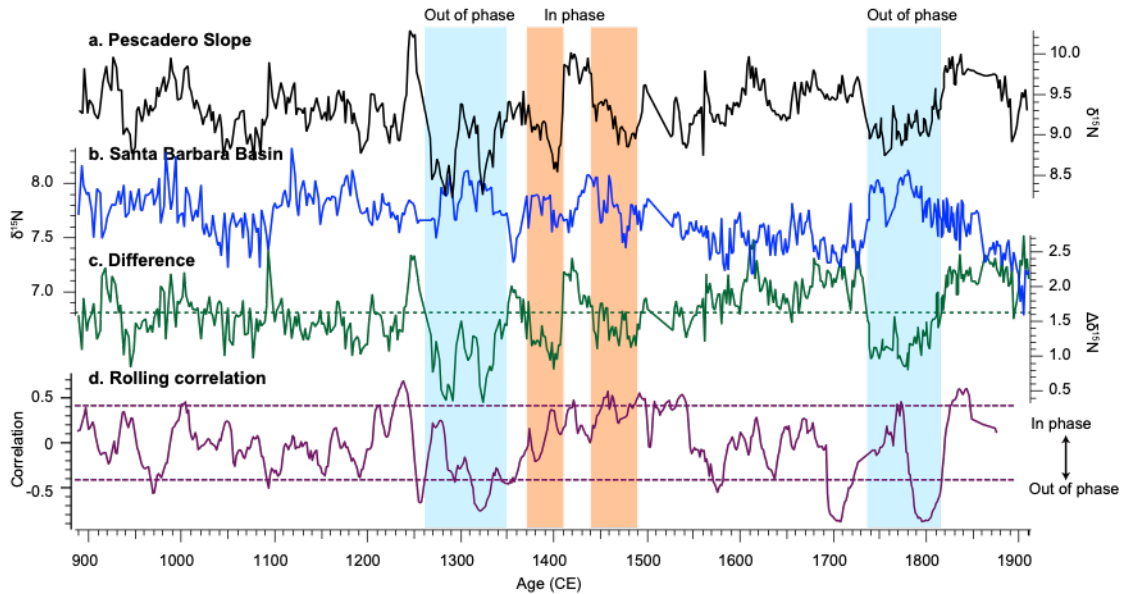


Figure S6. Comparison of $\Delta\delta^{15}N_{sed}$ ($\delta^{15}N_{sed}$ difference) and in-phase/out-of-phase $\delta^{15}N$ relationships. (a–b) Pescadero slope and Santa Barbara Basin $\delta^{15}N$ records, respectively. (c) $\Delta\delta^{15}N_{sed}$ between the two sites following Tems et al. (2015). The green dashed line shows the average value. (d) 25-point rolling correlation between the two sites. The two purple dashed lines show the threshold of statistically significant correlation coefficient at the 95% confidence level. Positive and negative correlation values indicate in phase and out-of-phase relationships, respectively. The blue bar shows an example interval with lower than average $\Delta\delta^{15}N_{sed}$ values under out-of-phase relationships.

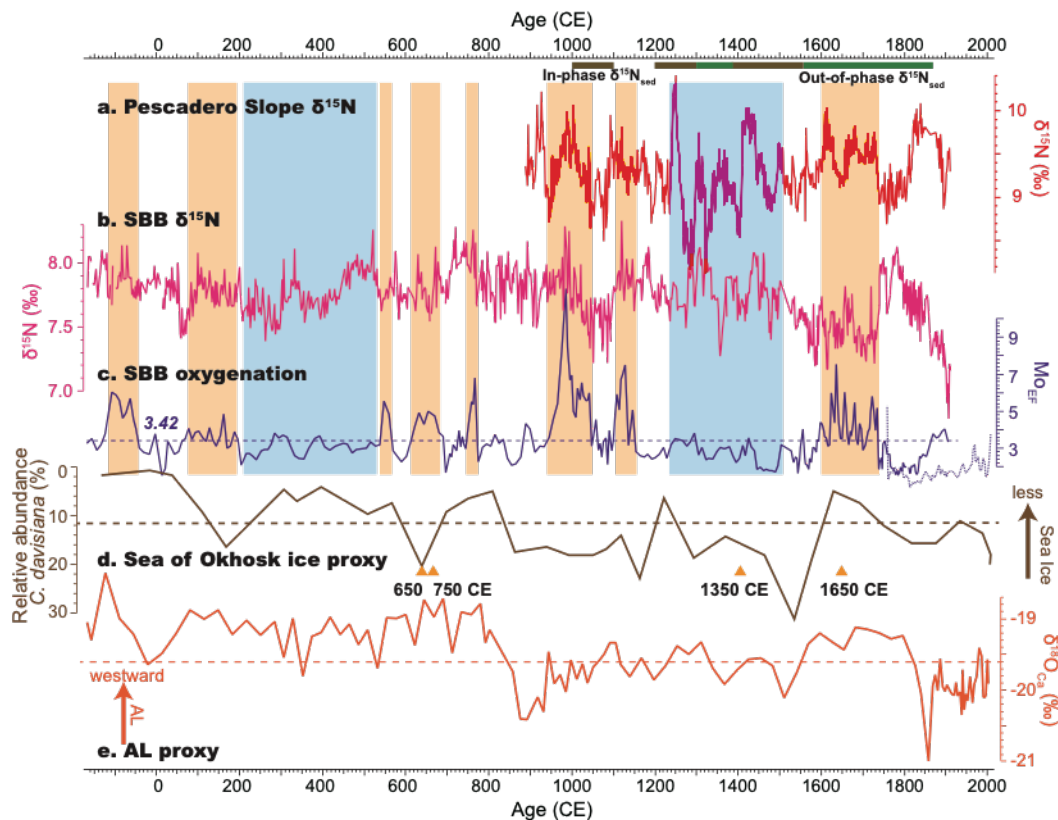


Figure S7. Extended record comparison that includes the first millennium for Fig. 3. (a) Bulk sedimentary $\delta^{15}\text{N}$ (red line) from the Pescadero slope (PESC-GC3; Tems et al. (2016)). We only focus on the last millennium in the main text due to the insufficient length of this record. (b) Bulk sedimentary $\delta^{15}\text{N}$ (pink line) from the SBB (SPR0901-03KC; Wang et al. (2019)). (c) Mo (purple line) enrichment factors for core SPR0901-03KC (solid) and SPR0901-04BC (dashed line) (Wang et al., 2017). (d) Relative abundance of *Cycladophora Davisiana* (brown line) in the Sea of Okhotsk (Itaki, 2004). The scale is inverted so high values (down) represent better ventilation. Orange triangles represent mollusca-based ^{14}C age control points; (e) Lake sediment carbonate $\delta^{18}\text{O}$ (orange line) in the Jellybean Lake (Anderson et al., 2005); Shaded bars represent 'more oxygen' (blue, defined with below average Mo_{EF} values) and 'low oxygen' (orange, defined with above average Mo_{EF} values). In-phase (brown bar at the top) and out-of-phase (green bar) relationships are determined using 25-point rolling correlation (Supplementary Information Text S5 and Fig. S5).

Table S1. Sediment reference material (MESS-3, PACS-2, and HISS-1) measurements.

Standard reference materials	Major elements	Certified (\pm SD)	Observed (\pm SD)
MESS-3 (n=23)	Al (%)	8.59 \pm 0.23	7.92 \pm 0.84
	Ba (ppm)	–	953 \pm 104
	Mo (ppm)	2.78 \pm 0.07	2.38 \pm 0.18
	Re (ppb)	–	3.23 \pm 0.40
PACS-2 (n=9)	Al (%)	6.62 \pm 0.32	6.24 \pm 0.46
	Ba (ppm)	–	894 \pm 81.8
	Mo (ppm)	5.43 \pm 0.28	4.79 \pm 0.50
	Re (ppb)	–	5.07 \pm 0.61
HISS-1 (n=9)	Al (%)	0.73 \pm 0.05	0.69 \pm 0.06
	Ba (ppm)	–	168.0 \pm 29.7
	Mo (ppm)	(0.13)	0.11 \pm 0.04

Table S2. Elemental compositions of SPR0901-03KC.

This table is uploaded in a separate file.

References

- Altabet, M.A. et al., 1999. The nitrogen isotope biogeochemistry of sinking particles from the margin of the Eastern North Pacific. *Deep Sea Research I*, 46(1999): 655-679.
- Berelson, W.M. et al., 2005. Anaerobic diagenesis of silica and carbon in continental margin sediments: Discrete zones of TCO₂ production. *Geochimica et Cosmochimica Acta*, 69(19): 4611-4629.
- Bishop, J.K.B., 1988. The barite-opal-organic carbon association in oceanic particulate matter. *Nature*, 332(6162): 341-343.
- Bostock, H.C., Opdyke, B.N., Williams, M.J.M., 2010. Characterising the intermediate depth waters of the Pacific Ocean using $\delta^{13}\text{C}$ and other geochemical tracers. *Deep Sea Research Part I: Oceanographic Research Papers*, 57(7): 847-859.
- Dymond, J., Suess, E., Lyle, M., 1992. Barium in Deep-Sea Sediment: A Geochemical Proxy for Paleoproductivity. *Paleoceanography*, 7(2): 163-181.
- Eagle, M., Paytan, A., Arrigo, K.R., van Dijken, G., Murray, R.W., 2003. A comparison between excess barium and barite as indicators of carbon export. *Paleoceanography*, 18(1).
- Ganeshram, R.S., François, R., Commeau, J., Brown-Leger, S.L., 2003. An experimental investigation of barite formation in seawater. *Geochimica et Cosmochimica Acta*, 67(14): 2599-2605.
- Gingele, F.X., Zabel, M., Kasten, S., Bonn, W.J., Nürnberg, C.C., 1999. Biogenic Barium as a Proxy for Paleoproductivity: Methods and Limitations of Application. In: Fischer, G., Wefer, G. (Eds.), *Use of Proxies in Paleoceanography: Examples from the South Atlantic*. Springer Berlin Heidelberg, Berlin, Heidelberg, pp. 345-364.
- Griffith, E.M., Paytan, A., 2012. Barite in the ocean - occurrence, geochemistry and palaeoceanographic applications. *Sedimentology*, 59(6): 1817-1835.
- Hakim, G.J. et al., 2016. The last millennium climate reanalysis project: Framework and first results. *Journal of Geophysical Research: Atmospheres*, 121(12): 6745-6764.

- Hamill, T.M., Whitaker, J.S., Snyder, C., 2001. Distance-Dependent Filtering of Background Error Covariance Estimates in an Ensemble Kalman Filter. *Monthly Weather Review*, 129(11): 2776-2790.
- Harrison, B.K., Zhang, H., Berelson, W., Orphan, V.J., 2009. Variations in archaeal and bacterial diversity associated with the sulfate-methane transition zone in continental margin sediments (Santa Barbara Basin, California). *Appl Environ Microbiol*, 75(6): 1487-99.
- Hendy, I.L., 2010. Diagenetic behavior of barite in a coastal upwelling setting. *Paleoceanography*, 25(4).
- Kienast, S.S., Calvert, S.E., Pedersen, T.F., 2002. Nitrogen isotope and productivity variations along the northeast Pacific margin over the last 120 kyr: Surface and subsurface paleoceanography. *Paleoceanography*, 17(4): 7-1-7-17.
- Kimura, N., 2004. Increase and decrease of sea ice area in the Sea of Okhotsk: Ice production in coastal polynyas and dynamic thickening in convergence zones. *Journal of Geophysical Research*, 109(C9).
- Kuwabara, J.S., Geen, A.V., Mccorkle, D.C., Bernhard, J.M., 1999. Dissolved sulfide distributions in the water column and sediment pore waters of the Santa Barbara Basin. *Geochimica et Cosmochimica Acta*, 63(15): 2199-2209.
- Liu, K.-K., Kaplan, I.R., 1989. The eastern tropical Pacific as a source of ^{15}N -enriched nitrate in seawater off southern California. *Limnology and Oceanography*, 34(5): 820-830.
- Martin, S., Drucker, R., Yamashita, K., 1998. The production of ice and dense shelf water in the Okhotsk Sea polynyas. *Journal of Geophysical Research: Oceans*, 103(C12): 27771-27782.
- McManus, J. et al., 1998. Geochemistry of barium in marine sediments: implications for its use as a paleoproxy. *Geochimica et Cosmochimica Acta*, 62(21): 3453-3473.
- McManus, J., Berelson, W.M., Klinkhammer, G.P., Kilgore, T.E., Hammond, D.E., 1994. Remobilization of barium in continental margin sediments. *Geochimica et Cosmochimica Acta*, 58(22): 4899-4907.
- Miyao, T., Ishikawa, K., 2003. Formation, distribution and volume transport of the North Pacific Intermediate Water studied by repeat hydrographic observations. *Journal of Oceanography*, 59(6): 905-919.
- PAGES 2k Consortium, 2017. A global multiproxy database for temperature reconstructions of the Common Era. *Sci Data*, 4: 170088.
- Parkinson, C.L., 1990. The Impact of the Siberian High and Aleutian Low on the Sea-Ice Cover of the Sea of Okhotsk. *Annals of Glaciology*, 14: 226-229.
- Paytan, A., Griffith, E.M., 2007. Marine barite: Recorder of variations in ocean export productivity. *Deep Sea Research Part II: Topical Studies in Oceanography*, 54(5-7): 687-705.
- Raven, M.R., Sessions, A.L., Fischer, W.W., Adkins, J.F., 2016. Sedimentary pyrite $\delta^{34}\text{S}$ differs from porewater sulfide in Santa Barbara Basin: Proposed role of organic sulfur. *Geochimica et Cosmochimica Acta*, 186: 120-134.
- Reid, J.L., 1965. Intermediate waters of the Pacific Ocean. *Johns Hopkins Oceanography Studies*, 5: 1-96.
- Reimers, C.E., Ruttenberg, K.C., Canfield, D.E., Christiansen, M.B., Martin, J.B., 1996. Porewater pH and authigenic phases formed in the uppermost sediments of the Santa Barbara Basin. *Geochimica et Cosmochimica Acta*, 60(21): 4037-4057.
- Riedinger, N., Kasten, S., Gröger, J., Franke, C., Pfeifer, K., 2006. Active and buried authigenic barite fronts in sediments from the Eastern Cape Basin. *Earth and Planetary Science Letters*, 241(3-4): 876-887.
- Shcherbina, A.Y., Talley, L.D., Rudnick, D.L., 2004a. Dense water formation on the northwestern shelf of the Okhotsk Sea: 1. Direct observations of brine rejection. *Journal of Geophysical Research: Oceans*, 109(C9).

- Shcherbina, A.Y., Talley, L.D., Rudnick, D.L., 2004b. Dense water formation on the northwestern shelf of the Okhotsk Sea: 2. Quantifying the transports. *Journal of Geophysical Research: Oceans*, 109(C9).
- Steiger, N.J., Hakim, G.J., Steig, E.J., Battisti, D.S., Roe, G.H., 2014. Assimilation of Time-Averaged Pseudoproxies for Climate Reconstruction. *Journal of Climate*, 27(1): 426-441.
- Tachibana, Y., Honda, M., Takeuchi, K., 1996. The Abrupt Decrease of the Sea Ice over the Southern Part of the Sea of Okhotsk in 1989 and Its Relation to the Recent Weakening of the Aleutian Low. *Journal of the Meteorological Society of Japan. Ser. II*, 74(4): 579-584.
- Talley, L.D., 1993. Distribution and formation of North Pacific Intermediate Water. *Journal of Geophysical Oceanography*, 23: 517-537.
- Tardif, R. et al., 2019. Last Millennium Reanalysis with an expanded proxy database and seasonal proxy modeling. *Climate of the Past*, 15(4): 1251-1273.
- Taylor, K.E., Stouffer, R.J., Meehl, G.A., 2011. An Overview of CMIP5 and the Experiment Design. *Bulletin of the American Meteorological Society*, 93(4): 485-498.
- Tems, C.E., Berelson, W.M., Prokopenko, M.G., 2015. Particulate $\delta^{15}\text{N}$ in laminated marine sediments as a proxy for mixing between the California Undercurrent and the California Current: A proof of concept. *Geophysical Research Letters*, 42(2): 419-427.
- Tems, C.E. et al., 2016. Decadal to centennial fluctuations in the intensity of the eastern tropical North Pacific oxygen minimum zone during the last 1200 years. *Paleoceanography*, 31(8): 1138-1151.
- Torres, M.E., Brumsack, H.J., Bohrmann, G., Emeis, K.C., 1996. Barite fronts in continental margin sediments: a new look at barium remobilization in the zone of sulfate reduction and formation of heavy barites in diagenetic fronts. *Chemical Geology*, 127(1): 125-139.
- Von Breyman, M.T., Emeis, K.-C., Suess, E., 1992. Water depth and diagenetic constraints on the use of barium as a palaeoproductivity indicator. *Geological Society, London, Special Publications*, 64(1): 273.
- Wang, Y., Hendy, I.L., Thunell, R., 2019. Local and Remote Forcing of Denitrification in the Northeast Pacific for the Last 2,000 Years. *Paleoceanography and Paleoclimatology*.
- Watanabe, T., Wakatsuchi, M., 1998. Formation of 26.8–26.9 σ_{θ} water in the Kuril Basin of the Sea of Okhotsk as a possible origin of North Pacific Intermediate Water. *Journal of Geophysical Research: Oceans*, 103(C2): 2849-2865.
- Yasuda, I., 1997. The origin of the North Pacific Intermediate Water. *Journal of Geophysical Research*, 102(C1): 893.
- You, Y., 2003. The pathway and circulation of North Pacific Intermediate Water. *Geophysical Research Letters*, 30(24).
- You, Y. et al., 2000. Roles of the Okhotsk Sea and Gulf of Alaska in forming the North Pacific Intermediate Water. *Journal of Geophysical Research*, 105(C2): 3253.
- You, Y. et al., 2003. Transport of North Pacific Intermediate Water across Japanese WOCE sections. *Journal of Geophysical Research*, 108(C6).